



**HAL**  
open science

## Allochthonous material originating from saprolite as a marker of termite activity in Ferralsols

Ary Bruand, Adriana Reatto, Éder de Souza Martins

### ► To cite this version:

Ary Bruand, Adriana Reatto, Éder de Souza Martins. Allochthonous material originating from saprolite as a marker of termite activity in Ferralsols. *Scientific Reports*, 2022, 12 (1), pp.17193. 10.1038/s41598-022-21613-6 . insu-03819381

**HAL Id: insu-03819381**

**<https://insu.hal.science/insu-03819381v1>**

Submitted on 18 Oct 2022

**HAL** is a multi-disciplinary open access archive for the deposit and dissemination of scientific research documents, whether they are published or not. The documents may come from teaching and research institutions in France or abroad, or from public or private research centers.

L'archive ouverte pluridisciplinaire **HAL**, est destinée au dépôt et à la diffusion de documents scientifiques de niveau recherche, publiés ou non, émanant des établissements d'enseignement et de recherche français ou étrangers, des laboratoires publics ou privés.



Distributed under a Creative Commons Attribution 4.0 International License



OPEN

## Allochthonous material originating from saprolite as a marker of termite activity in Ferralsols

Ary Bruand<sup>1✉</sup>, Adriana Reatto<sup>2</sup> & Éder de Souza Martins<sup>3</sup>

Ferralsols, which are estimated to cover 7.5 millions km<sup>2</sup> worldwide, are deeply weathered red or yellow soils found in the humid tropics. They are considered as the end of a geochemical sequence of weathering and are dominated by low-activity clay and sesquioxides. Their physical properties are closely related to their strong submillimetric granular structure. We aimed to characterize the 2:1 clay minerals identified in many Ferralsols and to discuss them as a marker of soil-feeding termite activity in Ferralsols. We present results recorded with Brazilian Ferralsols developed under Cerrado native vegetation on a range of parent materials. It was found that the 2:1 minerals vary from weakly weathered muscovite to hydroxy-Al interlayered vermiculite, sometimes associated to a fine material with a chemical composition highly different from that of the groundmass of the surrounding submillimetric granular aggregates. Results show that both 2:1 minerals and the associated fine material have to be considered as allochthonous material originating from the saprolite and were brought to the Ferralsol by soil-feeding termite activity. This confirms the major role of termites in the properties of Ferralsols and raises questions about the possible consequences of land use change which usually deeply affects soil biodiversity.

Ferralsols are the deeply weathered red or yellow soils found in the humid tropics<sup>1</sup>. These soils show a poor horizons with very diffuse limits between horizons. They are dominated by low-activity clay (mainly kaolinite) and a high sesquioxide content. They are considered as the end of a geochemical sequence of weathering<sup>2–4</sup> and most show a weak macrostructure and strong submillimetric granular structure<sup>5–9</sup>. As indicated in the World Reference Base for soil resources<sup>1</sup>, Ferralsols often refer to Oxisols (United States of America), Latossolos (Brazil), Kandosols (Australia), Ferralitic soils (Russia), sols ferrallitiques or Ferrallisols (France) and Ferralítico, Alítico and Ferrilítico (Cuba). Their worldwide extent is estimated at 7.5 million km<sup>2</sup>. They are mainly developed on materials resulting from long and deep weathering of the rocks forming the continental shields of South America (Brazil) and Africa (Congo, Democratic Republic of the Congo, Angola, Guinea, southern Central Africa and Eastern Madagascar). Outside these regions, Ferralsols can be found in areas with easily weathered basic rocks and both a hot and wet climate such as Southern Asia<sup>1</sup>. In South America, Ferralsols are numerous and developed on a large range of parent materials in the Cerrado biome (2.1 million km<sup>2</sup>) where they represent 49% of the surface area<sup>10</sup>. Their possible degradation following native vegetation clearing and then agricultural development with its consequences on soil biodiversity is often questioned<sup>11–14</sup>.

Although the submillimetric granular structure has long been recognized in most Ferralsols as responsible for most of their physical fertility, its origin remains highly debated<sup>7,15–18</sup>. An increasing numbers of studies, however, favor a structure resulting from long term soil faunal activity, particularly soil-feeding termite activity<sup>7,17–21</sup>. This hypothesis has been mainly discussed for Brazilian Ferralsols where termites communities are abundant and where 2:1 clay minerals have been observed in the ferralic B horizons in contradiction with the geochemical evolution of the soils<sup>7,20,22</sup>. This is a major issue because if both the submillimetric granular structure and the presence of 2:1 clay minerals result from the action of soil-feeding termites under native vegetation, its clearing the vegetation to allow the development of intensive agriculture will cause a collapse of the soil biodiversity, as has been shown for other tropical native vegetations in Africa with a dramatic decrease in the number of soil-feeding termite species<sup>22–24</sup>. This has potentially dramatic consequences for the physical and chemical fertility

<sup>1</sup>Institut des Sciences de la Terre d'Orléans (ISTO), UMR7327, UO-CNRS-BRGM, Observatoire des Sciences de l'Univers en région Centre, Université d'Orléans, 1A rue de la Férollerie, 45071 Orléans, Cedex 2, France. <sup>2</sup>Empresa Brasileira de Pesquisa Agropecuária (Embrapa), Secretaria de Pesquisa e Desenvolvimento, Parque Estação Biológica-PqEB S/n0, Brasília, DF, Brazil. <sup>3</sup>Empresa Brasileira de Pesquisa Agropecuária (Embrapa Cerrados), Brasília, DF, Brazil. ✉email: Ary.Bruand@univ-orleans.fr

of millions of hectares of Ferralsols that are physically fragile and chemically highly depleted due to their long and intense geochemical weathering<sup>2–4</sup>.

## Results and discussion

**Widespread presence of 2:1 clay minerals in ferralic B horizons.** In this study, we looked for evidence of the presence of material originating from the saprolite in the ferralic B horizons of Brazilian Ferralsols where termites were suspected to bring saprolite material from the soil bottom<sup>7,18,25</sup>. These soils are good candidates for highlighting the presence of material originating from the saprolite which usually appears usually at several meters depth, as the mineralogical composition of their ferralic B horizons is very different from that of the underlying saprolite. Moreover, they host numerous soil-feeding termite communities<sup>7,20,26–30</sup>.

The backscattered electron scanning images (BESI) and maps of K content (Fig. 1), as well as the point chemical analyses carried out (Supplementary Table 1), showed that elongated particles with a K<sub>2</sub>O content ranging from 0.50 (Fig. 1e) to 10.87% (Fig. 1g) (Supplementary Table 1) were present in the ferralic B horizons of the four Ferralsols studied (“Methods”). According to earlier results, these elongated particles are 2:1 clay particles<sup>18</sup>. They ranged from a few microns in length belonging to the large clay- or fine silt-size fraction (Fig. 1c,d,g,h) to several hundred microns in length belonging to the fine sand-size fraction (Fig. 1a,b). Thus, they can be much larger than those evidenced earlier in Ferralsols<sup>18</sup>. Observation of the whole surface area of the polished cross section (“Methods”) showed that clay-size elongated particles (< 2 μm long) with a K<sub>2</sub>O content > 0.5% were highly numerous (i.e. > 50 particles for the 4.9 cm<sup>2</sup> observed) in the Ferralsols F1, F2 and F3 and numerous (i.e. 10 to 50 particles for the 4.9 cm<sup>2</sup> observed) in the Ferralsol F4 (Table 1). Fine silt-size particles (2–20 μm long) were highly numerous in F1 and F3 and numerous in F2 and F4 (Table 1). Similar large silt-size particles (20–50 μm long) were highly numerous only in F3, numerous in F1, poorly present (i.e. 1 to 10 particles for the 4.9 cm<sup>2</sup> observed) in F2 and not observed in F4 (Table 1). Lastly, fine sand-size particles (50–500 μm long) were numerous in F1 and poorly present in F3 (Table 1). Thus, even if the elongated particles showing an internal structure of phyllosilicates varied in size, in abundance in the groundmass fabric of the submillimetric granular aggregates and in K<sub>2</sub>O content, they were present in the four ferralic B horizons studied and corresponded to the 2:1 clay minerals identified earlier using XR diffraction but without having the possibility to describe their morphology and to determine their chemical composition<sup>29,31–37</sup>.

The structural formula was computed for these 2:1 clay minerals on the basis of the structure of a 2:1 phyllosilicate. The results recorded for the analyses exhibiting the highest K<sub>2</sub>O content among the analyses performed (Fig. 1, Supplementary Table 1) and after attributing all Mg<sup>2+</sup> to the octahedral sites showed that the number of occupied sites in the octahedral sheet ranged from 2.01 to 2.05 for the half unit cell in F1, F3 and F4 (Table 2). The electrical charge of the sheet for the half unit ranged from – 1.02 to – 1.03 and the electrical charge corresponding to the cations K<sup>+</sup>, Ca<sup>2+</sup> and Na<sup>+</sup> in the interlayer space from + 0.89 to + 0.97 (Table 2).

Comparison of the Al<sub>2</sub>O<sub>3</sub>, SiO<sub>2</sub> and K<sub>2</sub>O + Na<sub>2</sub>O + CaO contents recorded for the elongated particles observed in F1, F2, F3 and F4 with their respective contents in a theoretical muscovite, an unweathered muscovite and a highly weathered muscovite showed that the chemical compositions recorded for the fine sand-size elongated particle shown in Fig. 1a and for the other elongated particles showing the highest K<sub>2</sub>O content (Fig. 1e,f, Supplementary Table 1) were close to those of the theoretical muscovite and unweathered muscovite (Fig. 2a). Figure 2a shows also that the zonation observed on the BESI of the particle analyzed in F3 and the map of its K<sub>2</sub>O content corresponded to a variation in the chemical composition between a weakly weathered muscovite and a deeply weathered muscovite. Lastly, the small-size elongated particles analyzed in Fig. 1c showed a smaller SiO<sub>2</sub> content. This can be attributed to the fact that the particles analyzed were so small that the analysis partly included partly the surrounding groundmass material. This explains their location in the triangle showing the Al<sub>2</sub>O<sub>3</sub>, SiO<sub>2</sub> and K<sub>2</sub>O + Na<sub>2</sub>O + CaO contents (Fig. 2a). Globally, the increase in the Al<sub>2</sub>O<sub>3</sub> content when the K<sub>2</sub>O decreased has to be considered as the result of the intercalation of hydroxy-Al in the inter-layer space during the weathering process of the muscovite particles<sup>18</sup> leading to the formation of hydroxy-Al interlayered vermiculites (HIV) as shown by several authors<sup>29,31–37</sup>.

The BESI of F1 showed the presence of many large fine sand-size elongated particles with phyllosilicate morphology similar to the particle shown in Fig. 1a (Supplementary Fig. 1, Table 1). They all exhibited an internal layer organization with some large inter-layer spaces resulting from swelling properties, depending on the chemical composition of the 2:1 layers. The collapse of most inter-layer spaces when drying to the benefit of the greater opening of some inter-layer spaces explains the large inter-layer spaces observed. The K<sub>2</sub>O content in these fine sand-size elongated particles ranged from 7.51 to 11.24% (Supplementary Fig. 1, Supplementary Table 2). Comparison of the Al<sub>2</sub>O<sub>3</sub>, SiO<sub>2</sub> and K<sub>2</sub>O + Na<sub>2</sub>O + CaO mean contents recorded for these sand-size elongated particles and their respective contents in a theoretical muscovite and a natural unweathered muscovite showed that they were particles of very weakly weathered muscovite which can only originate from the underlying saprolite present from 300 cm depth (“Methods”) (Fig. 2b). The groundmass chemical composition (Fig. 2b, Supplementary Table 2) surrounding these sand-size particles is consistent with a mineralogical composition dominated by gibbsite as reported earlier for F1<sup>38</sup>, thus emphasizing the allochthonous character of the muscovite particles. We also computed the structural formula for these 2:1 clay minerals on the basis of the structure of a 2:1 phyllosilicate (Table 2). Results showed a very similar chemical composition of the half unit cell for the six particles analyzed, thus indicating that they originated from a saprolite containing a single type of muscovite with Na<sup>+</sup> in the interlayer space representing from 17 to 30% of the interlayer electrical charge (Table 2).

**Allochthonous clay particles and associated fine material.** Some areas with a groundmass that included a high proportion of elongated particles with K<sub>2</sub>O content > 0.5% and showed a chemical composition highly different from that of the groundmass forming the main part of the ferralic B horizon were observed in F1

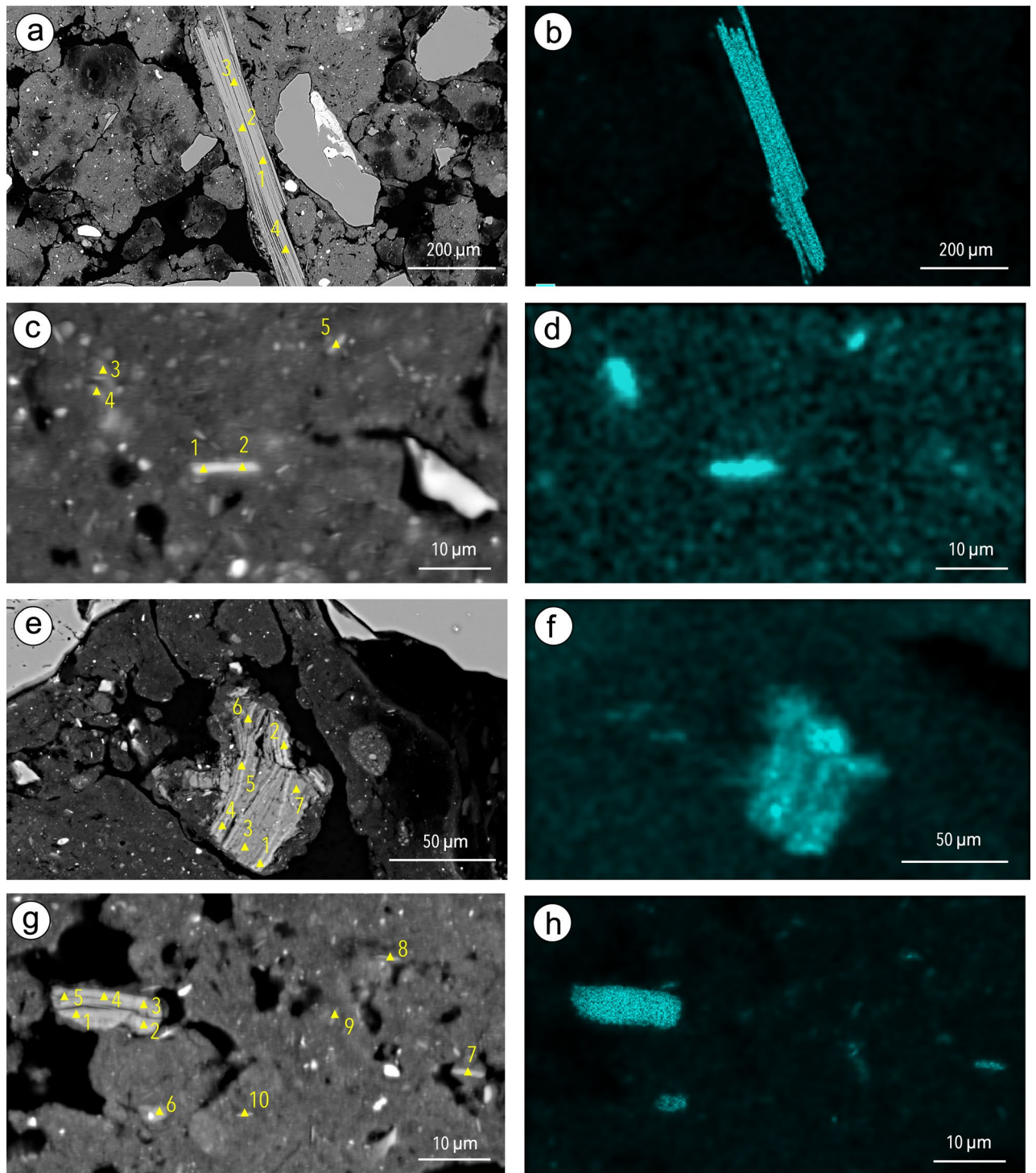


**Figure 1.** Elongated particles with varying sizes observed on the backscattered scanning images (BESI) of the cross sections of Ferralsols F1 (a), F2 (c), F3 (e) and F4 (g), location of the analyses (yellow triangles) performed by using energy dispersive spectrometry (EDS) (the numbers correspond to the analysis points in Supplementary Table 1), and K maps of the same areas using EDS for F1 (b), F2 (d), F3 (f) and F4 (h).

and F3. An area associating a high number of elongated particles varying in size and  $K_2O$  content to fine material with a chemical composition highly different from that of the groundmass material of the neighboring microagregate was observed in F3 (Fig. 3, Supplementary Table 3). Some elongated particles showed a small mean  $K_2O$  content (0.26%) (Supplementary Table 3) and may correspond to kaolinite particles or to HIV particles in which most  $K^+$  was removed and replaced by hydroxylated  $Al^{3+}$  as discussed earlier<sup>18</sup>. The other elongated particles showed a varying  $K_2O$  content but always  $>0.5\%$  with a mean  $K_2O$  content of 2.80% (Fig. 3, Supplementary Table 3). The structural formulas computed for the analyses with the highest  $K_2O$  content showed fewer sub-



Ferralsol	Length and number of the elongated particles			
	< 2 μm	2–20 μm	20–50 μm	50–500 μm
F1	> 50	> 50	10–50	10–50
F2	> 50	10–50	1–10	n.o
F3	> 50	> 50	> 50	1–10
F4	10–50	10–50	n.o	n.o

**Table 1.** Length and number of elongated particles with K<sub>2</sub>O content > 0.5% which were observed on the BESI of the polished sections 4.9 cm<sup>2</sup> in surface area (diameter of 2.5 cm). *n.o.* not observed.

Ferralsol	Location of the particle	Analyses taken into account	Chemical composition of the half unit cell	Number of octahedral cavities occupied	Electrical charge of the layer	Electrical charge of the cations in the interlayer space
F1	Figure 1a	Points 1 to 4	[Si <sub>3.02</sub> Al <sub>0.98</sub> ]O <sub>10</sub> [Al <sub>1.81</sub> Fe <sub>0.10</sub> Mg <sub>0.07</sub> Ti <sub>0.03</sub> ](OH) <sub>2</sub> K <sub>0.72</sub> Ca <sub>0.00</sub> Na <sub>0.25</sub>	2.01	– 1.02	+ 0.97
F3	Figure 1e	Point 2	[Si <sub>3.00</sub> Al <sub>1.00</sub> ]O <sub>10</sub> [Al <sub>1.69</sub> Fe <sub>0.25</sub> Mg <sub>0.07</sub> Ti <sub>0.04</sub> ](OH) <sub>2</sub> K <sub>0.84</sub> Ca <sub>0.01</sub> Na <sub>0.06</sub>	2.02	– 1.03	+ 0.92
F4	Figure 1g	Points 1 to 5	[Si <sub>3.01</sub> Al <sub>0.99</sub> ]O <sub>10</sub> [Al <sub>1.82</sub> Fe <sub>0.16</sub> Mg <sub>0.05</sub> Ti <sub>0.02</sub> ](OH) <sub>2</sub> K <sub>0.78</sub> Ca <sub>0.01</sub> Na <sub>0.09</sub>	2.05	– 1.02	+ 0.89
F1	Supplementary Fig. 1a	Points 1 to 18	[Si <sub>3.07</sub> Al <sub>0.93</sub> ]O <sub>10</sub> [Al <sub>1.78</sub> Fe <sub>0.11</sub> Mg <sub>0.08</sub> Ti <sub>0.04</sub> ](OH) <sub>2</sub> K <sub>0.77</sub> Ca <sub>0.01</sub> Na <sub>0.15</sub>	2.01	– 0.97	+ 0.94
	Supplementary Fig. 1b	Points 1 to 12	[Si <sub>3.07</sub> Al <sub>0.93</sub> ]O <sub>10</sub> [Al <sub>1.81</sub> Fe <sub>0.10</sub> Mg <sub>0.06</sub> Ti <sub>0.04</sub> ](OH) <sub>2</sub> K <sub>0.69</sub> Ca <sub>0.01</sub> Na <sub>0.25</sub>	2.01	– 0.95	+ 0.96
	Supplementary Fig. 1c	Points 1 to 10	[Si <sub>3.06</sub> Al <sub>0.94</sub> ]O <sub>10</sub> [Al <sub>1.75</sub> Fe <sub>0.16</sub> Mg <sub>0.09</sub> Ti <sub>0.04</sub> ](OH) <sub>2</sub> K <sub>0.72</sub> Ca <sub>0.01</sub> Na <sub>0.15</sub>	2.04	– 0.99	+ 0.89
	Supplementary Fig. 1d	Points 1 to 9	[Si <sub>3.05</sub> Al <sub>0.95</sub> ]O <sub>10</sub> [Al <sub>1.82</sub> Fe <sub>0.10</sub> Mg <sub>0.05</sub> Ti <sub>0.03</sub> ](OH) <sub>2</sub> K <sub>0.67</sub> Ca <sub>0.00</sub> Na <sub>0.28</sub>	2.00	– 0.97	+ 0.95
	Supplementary Fig. 1e	Points 1 to 14	[Si <sub>3.09</sub> Al <sub>0.91</sub> ]O <sub>10</sub> [Al <sub>1.73</sub> Fe <sub>0.13</sub> Mg <sub>0.12</sub> Ti <sub>0.05</sub> ](OH) <sub>2</sub> K <sub>0.82</sub> Ca <sub>0.00</sub> Na <sub>0.12</sub>	2.03	– 0.98	+ 0.94
	Supplementary Fig. 1f	Points 1 to 9	[Si <sub>3.07</sub> Al <sub>0.93</sub> ]O <sub>10</sub> [Al <sub>1.74</sub> Fe <sub>0.13</sub> Mg <sub>0.10</sub> Ti <sub>0.05</sub> ](OH) <sub>2</sub> K <sub>0.79</sub> Ca <sub>0.00</sub> Na <sub>0.13</sub>	2.02	– 0.98	+ 0.92
F3	Figure 3c	Point 15	[Si <sub>3.21</sub> Al <sub>0.79</sub> ]O <sub>10</sub> [Al <sub>1.62</sub> Fe <sub>0.19</sub> Mg <sub>0.26</sub> Ti <sub>0.03</sub> ](OH) <sub>2</sub> K <sub>0.70</sub> Ca <sub>0.01</sub> Na <sub>0.01</sub>	2.10	– 1.02	+ 0.73
	Figure 3d	Point 1	[Si <sub>3.19</sub> Al <sub>0.81</sub> ]O <sub>10</sub> [Al <sub>1.56</sub> Fe <sub>0.24</sub> Mg <sub>0.30</sub> Ti <sub>0.02</sub> ](OH) <sub>2</sub> K <sub>0.71</sub> Ca <sub>0.01</sub> Na <sub>0.01</sub>	2.12	– 1.09	+ 0.74
F1	Supplementary Fig. 2	Points 1 to 6	[Si <sub>3.05</sub> Al <sub>0.95</sub> ]O <sub>10</sub> [Al <sub>1.81</sub> Fe <sub>0.11</sub> Mg <sub>0.06</sub> Ti <sub>0.03</sub> ](OH) <sub>2</sub> K <sub>0.69</sub> Ca <sub>0.01</sub> Na <sub>0.25</sub>	2.01	– 0.98	+ 0.96
	Theoretical muscovite <sup>60</sup>		[Si <sub>3.00</sub> Al <sub>1.00</sub> ]O <sub>10</sub> [Al <sub>2.00</sub> ](OH) <sub>2</sub> K <sub>1.00</sub>	2.00	– 1.00	+ 1.00
	Muscovite in a granite <sup>41</sup>		[Si <sub>3.16</sub> Al <sub>0.84</sub> ]O <sub>10</sub> [Al <sub>1.66</sub> Fe <sub>0.07</sub> Mg <sub>0.28</sub> Ti <sub>0.05</sub> ](OH) <sub>2</sub> K <sub>0.95</sub>	2.06	– 1.07	+ 0.95

**Table 2.** Chemical composition of the half unit cell computed after location of the whole Mg<sup>2+</sup> in the octahedral sites for the mean chemical composition resulting from the analyses of the particles varying in size shown in BESI of Fig. 1 and of the fine sand-size elongated particles shown in the BESI of Fig. 2. Chemical compositions of the half unit cell of a theoretical muscovite<sup>59</sup> and of a muscovite in a granite<sup>60</sup> are also given.

stitutions of Si<sup>4+</sup> by Al<sup>3+</sup> than recorded for the large particle shown in F3 (Fig. 1e, Table 2) and for all the other elongated particles analyzed (Table 2). The structural formulas computed are close to that of a natural muscovite (Table 2). And if we limit the number of octahedral sites occupied at two sites by distributing Mg<sup>2+</sup> between the octahedral sites and the interlayer space, the negative electrical charges of the layer (– 0.92 and – 0.91 for the two points analyzed) are better equilibrated with the positive electrical charges (+ 0.93 and + 0.96, respectively) resulting from the cations located within the interlayer space. As for the fine material closely associated to these elongated particles, its Al<sub>2</sub>O<sub>3</sub> and SiO<sub>2</sub> mean contents were 38.31 and 43.16%, respectively while they were

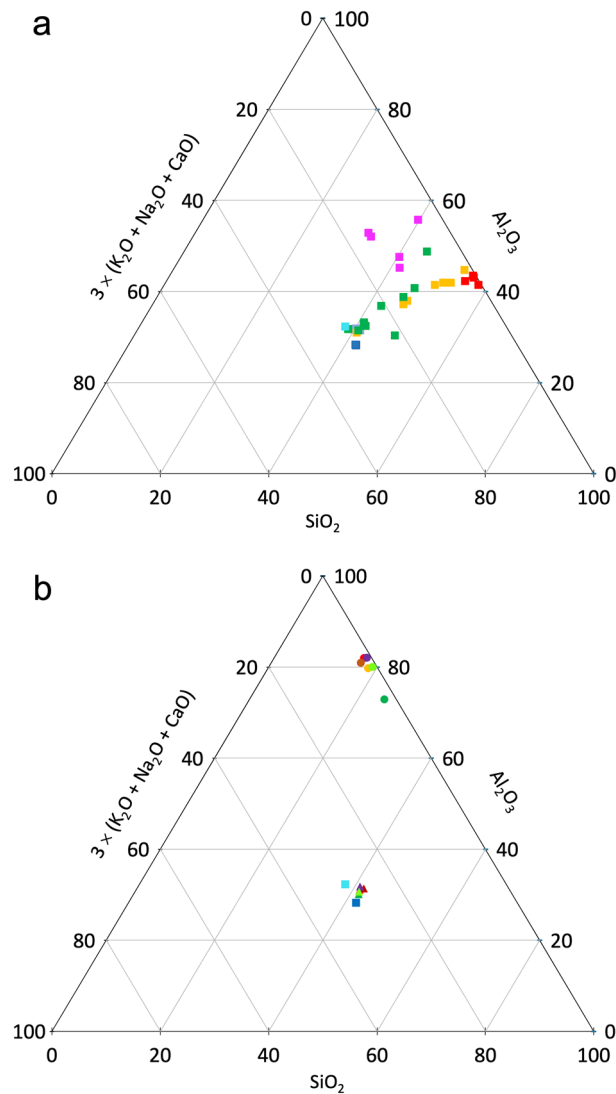


**Figure 2.** Respective content in  $\text{Al}_2\text{O}_3$ ,  $\text{SiO}_2$  and  $\text{K}_2\text{O} + \text{Na}_2\text{O} + \text{CaO}$  in the elongated particles varying in size shown in Ferralsols F1 (grey squares, Fig. 1a), F2 (purple squares, Fig. 1c), F3 (yellow squares, Fig. 1e) and F4 (green squares, Fig. 1g). Theoretical composition of muscovite (light blue square)<sup>59</sup>, composition of muscovite particles (deep blue squares)<sup>60</sup> and of weathered muscovite (red squares)<sup>60</sup> are also plotted.

48.83 and 27.39%, respectively for the groundmass material of the neighboring microaggregate (Supplementary Table 3).

In F1, small aggregates consisting of elongated particles with  $\text{K}_2\text{O}$  content  $> 0.5\%$  closely associated to fine material with a chemical composition highly different from that of the groundmass material of the surrounding submillimetric granular aggregates were present (Supplementary Fig. 2, Supplementary Table 4). While the  $\text{Al}_2\text{O}_3$  and  $\text{SiO}_2$  mean contents were 54.73 and 11.45%, respectively for the groundmass of the submillimetric granular aggregates (Supplementary Table 4), they were 43.71 and 28.16%, respectively, for the fine material associated to the elongated particles with  $\text{K}_2\text{O}$  content  $> 0.5\%$ . We also observed also a smaller  $\text{K}_2\text{O}$  content smaller in the groundmass material of the surrounding submillimetric granular aggregates (mean content of 0.11%) compared to that of the fine material (mean content of 1.34%) associated to the elongated particles with  $\text{K}_2\text{O}$  content  $> 0.5\%$  (Supplementary Fig. 2, Supplementary Table 4). We can hypothesize that in the fine material the  $\text{K}_2\text{O}$  content resulted from the presence of very small elongated particles of 2:1 clay minerals rich in  $\text{K}_2\text{O}$ . The structural formula computed was consistent with those already computed for the fine sand-size elongated particles which corresponded to weakly weathered muscovite (Table 2, Fig. 1a and Supplementary Fig. 1).

Thus, our results showed that fine material closely associated to the weathered muscovite particles had a smaller  $\text{Al}_2\text{O}_3$  content and a higher  $\text{SiO}_2$  content than the fine material composing the groundmass of the surrounding submillimetric granular aggregates observed in F1 and F3. These smaller  $\text{Al}_2\text{O}_3$  and higher  $\text{SiO}_2$  contents are additional arguments indicating that the muscovite particles and their associated fine material originate from the saprolite which is consistent with the geochemical sequence of weathering leading to the formation of Ferralsols<sup>2-4</sup> (Fig. 4). Hence, the presence of weathered muscovite particles and their associated fine material

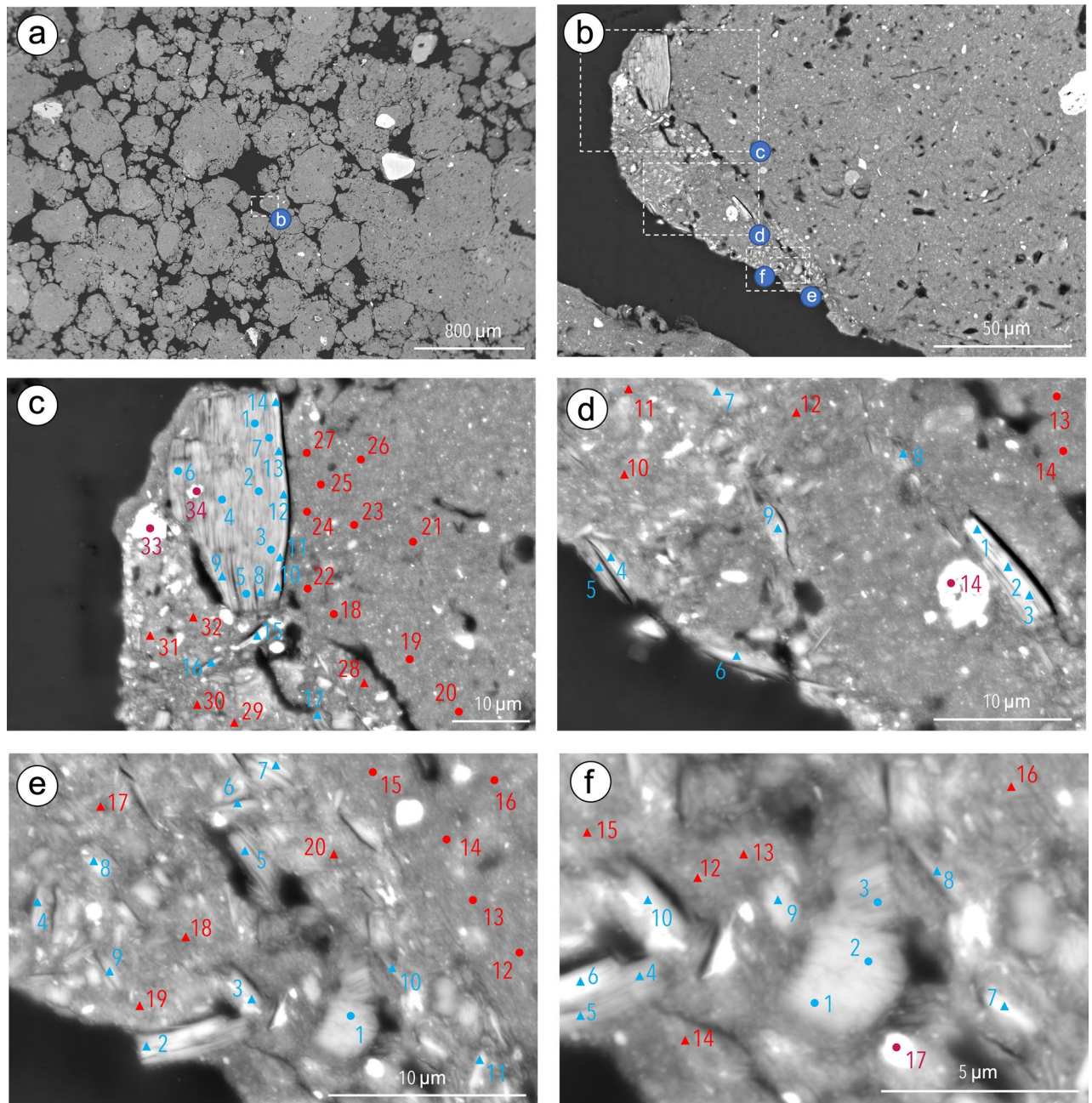


**Figure 3.** Location of an area with allochthonous material associated to the submillimetric granular aggregates (a) and of the four subareas where the analyses were performed (b) on the backscattered scanning images (BESI) of the cross sections of Ferralsols F3. Location of the analyses performed by using energy dispersive spectrometry (EDS) (c–f) in the particles with a small  $K_2O$  content (blue circles), the particles with a high  $K_2O$  content (blue triangles), their associated groundmass (red triangles), the groundmass of the surrounding submillimetric granular aggregates (red circles) and particles with a high  $Fe_2O_3$  content (deep red circles). The numbers correspond to the analysis points in Supplementary Table 3.

have to be considered as markers of soil-feeding termite activity. We can also infer, as has been hypothesized by several authors<sup>7,17,18,20,21,39</sup> (Fig. 4) that this ceaseless activity of soil-feeding termites consisting in fragmenting and reorganizing the soil is also the process responsible for the microaggregated structure of the Ferralsols.

### Implications

The implications of our results go far beyond the case of Ferralsols alone. If soil-feeding termites bring material from the underlying saprolite, usually located at several meters depth, up to the B horizons of Ferralsols, we can hypothesize that they bring similar material in all the horizons of Ferralsols and that they behave similarly for many other tropical soils<sup>6,40–42</sup>. In the latter, their potential contribution of material from the saprolite to the soil horizon is probably less visible than for Ferralsols due to a less sharp discontinuity in mineralogical composition



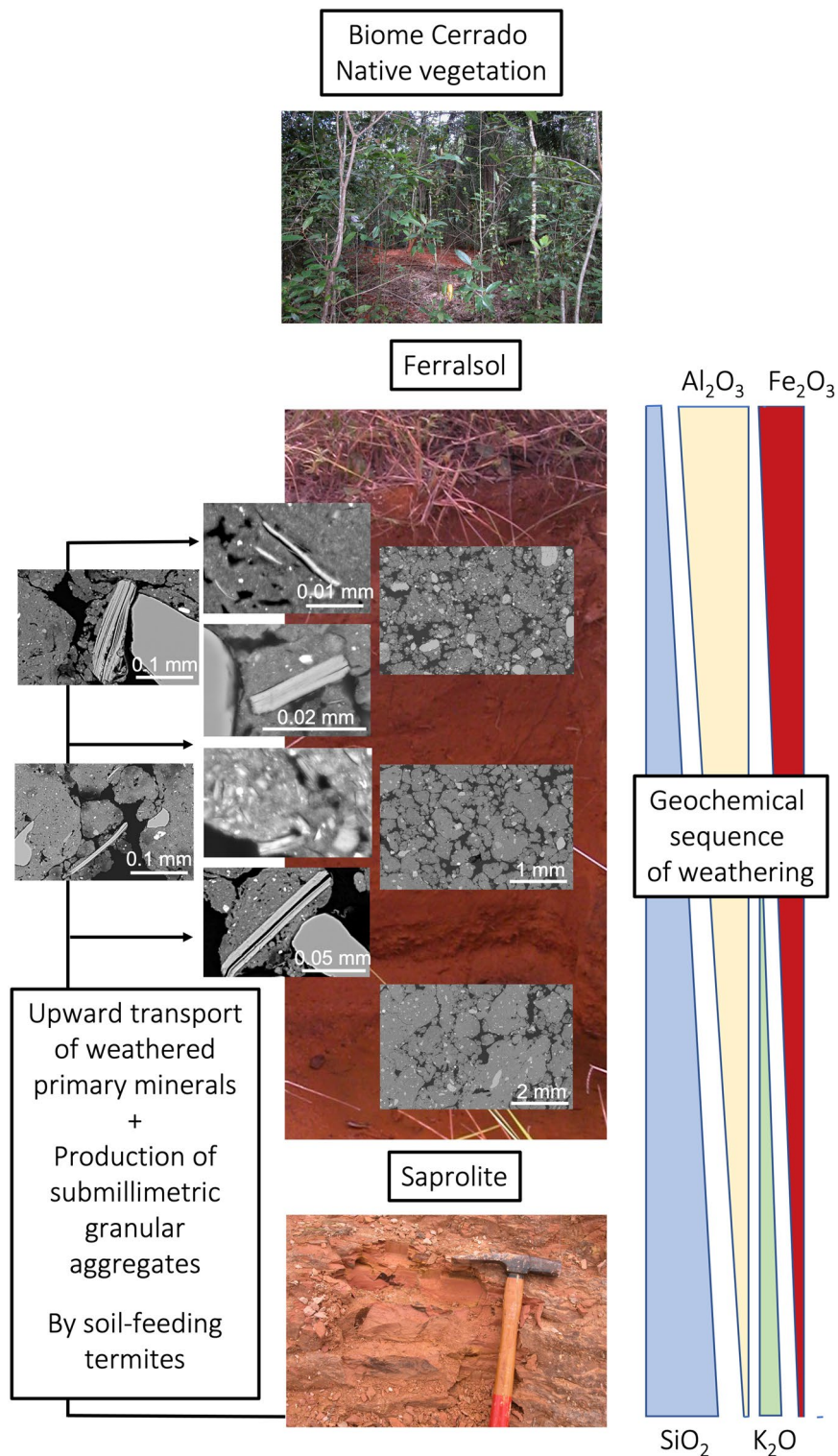


**Figure 4.** Synthetic diagram of the action of soil-feeding termites responsible for the presence of variably altered muscovite in the ferrallic B horizon of Ferralsols and of their submillimetric granular structure.

between the soil and the underlying saprolite. This contribution of soil-feeding termite activity to the soil characteristics is probably more frequent than is generally thought, which is in agreement with studies performed by soil biologists on the mineralogical composition of termite mounds and of the immediately surrounding soils<sup>19,40,43,44</sup>.

The presence of weathered muscovite particles resulting from soil-feeding termite activity constitutes a source of available  $K^+$  to plant nutrition in Ferralsols and is as such partly responsible for their chemical fertility. The weathered muscovite particles have to be considered as markers of the soil-feeding termite activity. Another



consequence of this activity is the submillimetric granular structure (Fig. 4) which is responsible for most of the physical properties of Ferralsols (e.g. water infiltration and retention, gas transfer properties, root penetration resistance). Consequently, when changes in land use occurs, more attention should be paid to possible changes affecting the soil-feeding termite communities<sup>12,14,45</sup>. Their contribution to both the physical and chemical properties of tropical soils is undoubtedly more important than is often acknowledged<sup>44–46</sup>. This is relevant to an issue currently under investigation by the scientific community, namely the consequences of the deforestation of savannas, particularly the sustainable management of these areas<sup>13,14,47</sup>.

## Methods

**The soils studied.** The Ferralsols studied are located in the Brazilian Central Plateau which presents two main geomorphologic surfaces: the Late Tertiary South American Surface (usually 900 to 1200 m high) which corresponds to tablelands where gibbsitic-sesquioxidic Ferralsols are dominant and the Late Quaternary Velhas Surface, which occurs 5 to 25 m below the South American Surface and shows a moderate slope where kaolinitic-non-sesquioxidic Ferralsols are numerous<sup>20,48–50</sup>. The most representative climate of the Brazilian Central Plateau is Megathermic or Humid Tropical (Aw) with the savanna subtype<sup>51</sup>. It is characterized by maximum rains in summer and a dry winter (average temperature of the coldest month > 18 °C). The average annual rainfall ranges from 1500 to 2000 mm, with the highest amounts of rainfall occurring in January and the lowest from June to August (< 50 mm per month)<sup>52</sup>. Four ferralic B horizons belonging to four Ferralsols were selected among Ferralsols studied earlier<sup>10,20,34,38,53–55</sup>. The four Ferralsols selected were located under native Cerrado, three on the Velhas Surface (F1, F3 and F4) and one the South American Surface (F2). F1 was collected in a Ferralsol (S 16°38'50.84" W 49°28'59.84") located at an elevation of 739 m and developed on a saprolite of a Precambrian mafic granulite<sup>56,57</sup> visible at a depth of 350 to 400 cm. The soil was originally recognized as being developed on the South American Surface<sup>53</sup> but further field analysis showed that it was developed on the Velhas Surface. This Ferralsol was studied earlier (soil L1)<sup>10,57</sup> and F1 corresponds to the horizon Bw<sub>2</sub> (100–160 cm) of Ferralsol classified as a gibbsitic-sesquioxidic Rhodic Ferralsol<sup>1</sup> ( $1.7 \times [\text{SiO}_2/\text{Al}_2\text{O}_3] = 0.4$ , Kaolinite/[Kaolinite + Gibbsite] = 0.3 and [Hematite/Hematite + Goethite] = 0.7). F2 was collected in a Ferralsol (S 15°36'3.20" W 47°44'1.48") located at an elevation of 1180 m and developed on a saprolite of a Precambrian quartzite<sup>56,57</sup> visible at a depth of 200 to 250 cm. This Ferralsol was studied earlier (soil L4)<sup>10,57</sup> and F2 corresponds to the horizon Bw<sub>1</sub> (60–110 cm) of this soil classified as a gibbsitic-sesquioxidic Plinthic Ferralsol<sup>1</sup> ( $1.7 \times [\text{SiO}_2/\text{Al}_2\text{O}_3] = 0.3$ , Kaolinite/[Kaolinite + Gibbsite] = 0.2 and [Hematite/Hematite + Goethite] = 0). F3 was collected in a Ferralsol (S 15°31'4.50" W 47°41'9.03") located at an elevation of 880 m and developed on a saprolite of a Precambrian metapelite where a lateritic crust is present<sup>56,57</sup> visible at a depth of 500 to 600 cm. This Ferralsol was studied earlier (soil L6)<sup>10,53</sup> and F3 corresponds to the horizon Bw<sub>2</sub> (140–200 cm) of a soil classified as kaolinitic-sesquioxidic Rhodic Ferralsol<sup>1</sup> ( $1.7 \times [\text{SiO}_2/\text{Al}_2\text{O}_3] = 0.8$ , Kaolinite/[Kaolinite + Gibbsite] = 0.5 and [Hematite/Hematite + Goethite] = 0.5). Finally, F4 was collected in a Ferralsol located in the Mato Grosso state at an elevation of 430 m (S 21°21'59.96" W 52°10'59.88") and developed on a saprolite of Cretaceous sandstones (Baurú group) visible at a depth of 300 to 350 cm<sup>54,55</sup>. This Bw horizon corresponds to the 60–110 cm horizon of a soil classified as a Rhodic Ferralsol<sup>1</sup>. The four ferralic B horizons selected show a weak macrostructure and a strong submillimetric granular structure<sup>10,54,55</sup>. The clay content of F1, F2, F3 and F4 was 520, 300, 780 and 782 g kg<sup>-1</sup>, respectively. Their cation exchange capacity was 2.0, 1.7, 10.0 and 2.5 cmol<sub>c</sub> kg<sup>-1</sup>, respectively with most exchangeable cations corresponding to H<sup>+</sup> and Al<sup>3+</sup><sup>53,54</sup>.

**Scanning electron microscopy and energy dispersive spectroscopy.** Undisturbed samples were collected with 100-cm<sup>3</sup> volume cylinders, dried and then included in a polyester resin<sup>58</sup>. After polymerization and hardening, circular cross sections 2.5 cm in diameter were prepared and carbon coated for examination in scanning electron microscopy (SEM) using backscattered electron scanning images (BESI). Observations were made from low magnifications ranging (35× to 200×) to high magnification ranging (1000× to 8000×) to identify particles of phyllosilicates in the groundmass<sup>18</sup>. The scanning electron microscope (SEM) used was a Merlin Compact Zeiss microscope (resolution of 0.8 nm at 15 kV and 1.6 nm at 1 kV; tension ranging from 20 V to 30 kV; probe current ranging from 12 pA to 100 nA). It was equipped with a Gemini I column including a backscattered electron detector (BSD) with five quadrants for acquisition of the backscattered electron scanning images (BESI). Observations were performed at 15 kV accelerating voltage and at a working distance of 10 mm. Chemical analyses were performed using energy dispersive X-ray spectroscopy (EDS) with a Quantax XFlash6 Bruker detector enabling a resolution of 129 eV. Analyses were performed also at 15 kV accelerating voltage. The SEM was operated with a resolution of 0.8 nm and a probe current of 1.6 nA. A count time of 100 s was used for punctual analyses. Total chemical composition was expressed on the basis that the sum of oxide mass equals 100 for determinations of SiO<sub>2</sub>, Al<sub>2</sub>O<sub>3</sub>, Fe<sub>2</sub>O<sub>3</sub>, MgO, CaO, K<sub>2</sub>O, and Na<sub>2</sub>O and TiO<sub>2</sub>. The chemical compositions were also plotted in ternary plots to show the Al<sub>2</sub>O<sub>3</sub>, SiO<sub>2</sub> and K<sub>2</sub>O + Na<sub>2</sub>O + CaO contents. Images of the concentration of K throughout the images were recorded with an acquisition time of 15 min.

## Data availability

The datasets used during the current study are available from the corresponding author on reasonable request.

Received: 7 July 2022; Accepted: 29 September 2022

Published online: 13 October 2022

## References

- IUSS Working Group WRB. World reference base for soil resources 2014, update 2015. International soil classification system for naming soils and creating legends for soil maps. World Soil Resources Reports No 106 (Food and Agricultural Organization, 2015).
- Melfi, A. J. & Pédro, G. Estudo geoquímico dos solos e formações superficiais do Brasil. Parte 1—Caracterização e repartição dos principais tipos de evolução pedogeológica. *R. Bras. Geosci.* **7**, 271–286 (1977).
- Melfi, A. J. & Pédro, G. Estudo geoquímico dos solos e formações superficiais do Brasil. Parte 2—Considerações sobre os mecanismos geoquímicos envolvidos na alteração superficial e sua repartição no Brasil. *R. Bras. Geoci.* **8**, 11–22 (1978).
- Pédro, G. Distribution des principaux types d'altération chimique à la surface du globe. *Rev. Géogr. Phys. Géol. Dyn.* **X**, 457–470 (1968).
- Stoops, G. Micromorphology of the oxyc horizon. In *Workshop Meeting on Soil Micromorphology* Vol. 2 (eds Bullock, P. & Murphy, C. P.) 419–440 (Academic Publisher, 1983).
- Trapnell, C. G. & Webster, R. Microaggregates in red earths and related soils in East and Central Africa, their classification and occurrence. *J. Soil Sci.* **37**, 109–123 (1986).
- Schaefer, C. E. G. R. Brazilian latosols and their B horizon microstructure as long-term biotic constructs. *Austr. J. Soil Res.* **39**, 909–926 (2001).
- Volland-Tuduri, N., Brossard, M., Bruand, A. & Garreau, H. Direct analysis of microaggregates shrinkage for drying: Application to microaggregates from a Brazilian clayey Ferralsol. *Comptes Rendus Géosci.* **336**, 1017–1024 (2004).
- Volland-Tuduri, N. *et al.* Mass proportion of microaggregates and bulk density in a Brazilian clayey Oxisol. *Soil Soc. Sci. Am. J.* **69**, 1559–1564 (2005).
- Reatto, A., Correia, J. R., Spera, S. T. & Martins, E. S. Solos do Bioma Cerrado : aspectos pedológicos. In *Ecologia e Flora* (eds Sano, S. *et al.*) 107–149 (Embrapa Informação Tecnológica, 2008).
- Gossner, M. M. *et al.* Land-use intensification causes multitrophic homogenization of grassland communities. *Nature* **540**(7632), 226 (2016).
- Strassburg, B. B. N., Latawiec, A. & Balmford, A. Urgent action on Cerrado extinctions. *Nature* **540**(7632), 199–199 (2016).
- Strassburg, B. B. N. *et al.* Moment of truth for the Cerrado hotspot. *Nat. Ecol. Evol.* **1**(4), 0099 (2017).
- Silva, C. H. L. *et al.* Northeast Brazil's imperiled Cerrado. *Science* **372**(6538), 139–140 (2021).
- Karathanasis, A. D., Adams, F. & Hajek, B. F. Stability relationships in kaolinite, gibbsite, and Al-hydroxyinterlayered vermiculite soil systems. *Soil Sci. Soc. Am. J.* **47**, 1247–1251 (1983).
- Cooper, M., Vidal-Torrado, P. & Chaplot, V. Origin of microaggregates in soils with ferralic horizons. *Sci. Agric.* **62**, 256–263 (2005).
- Marcelino, V., Schaefer, C. E. G. R. & Stoops, G. Oxidic and related material. In *Interpretations of Micromorphological Features of Soils and Regoliths* 2nd edn (eds Stoops, G. *et al.*) 663–689 (Elsevier B.V., 2018).
- Bruand, A. & Reatto, A. Morphology, chemical composition and origin of 2:1 phyllosilicates in Bw horizons of latosols of the Brazilian Central Plateau: Contribution to the discussion of the microgranular structure origin. *C.R. Geosci.* **354**, 159–185 (2022).
- Jouquet, P., Chintakunta, S., Bottinelli, N., Subramanian, S. & Caner, L. The influence of fungus-growing termites on soil macro and micro-aggregates stability varies with soil type. *Appl. Soil Ecol.* **101**, 117–123 (2016).
- Reatto, A. *et al.* Development and origin of the microgranular structure in Latosols of the Brazilian Central Plateau: Significance of texture, mineralogy and biological activity. *CATENA* **76**, 122–134 (2009).
- Lavelle, P. *et al.* Ecosystem engineers in a self-organized soil: A review of concepts and future research questions. *Soil Sci.* **181**, 91–109 (2016).
- Eggleton, P. *et al.* The diversity, abundance and biomass of termites under differing levels of disturbance in the Mbalmayo Forest Reserve, southern Cameroon. *Philos. Trans. R Soc. Lond. B* **351**(1335), 51–68 (1996).
- Lawton, J. H. *et al.* Biodiversity inventories, indicator taxa and effects of habitat modification in tropical forest. *Nature* **391**(6662), 72–76 (1998).
- Eggleton, P. *et al.* Termite diversity across an anthropogenic disturbance gradient in the humid forest zone of West Africa. *Agric. Ecosyst. Environ.* **90**, 189–202 (2002).
- Martinez, P. & Souza, I. F. Genesis of pseudo-sand structure in Oxisols from Brazil. A review. *Geoderma Reg.* **22**, e00292 (2020).
- Benito, N. P., Brossard, M., Pasini, A., Guimaraes, M. D. & Bobillier, B. Transformation of soil macroinvertebrate populations after native vegetation conversion to pasture cultivation (Brazilian Cerrado). *Eur. J. Biol.* **40**, 147–154 (2004).
- Sarcinelli, T. S. *et al.* Chemical, physical and micromorphological properties of termite mounds and adjacent soils along a toposequence in Zona da Mata, Minas Gerais State, Brazil. *CATENA* **76**, 107–113 (2009).
- Sarcinelli, T. S., Schaefer, C. E. G. R., Fernandes, E. I., Mafia, R. G. & Neri, A. V. Soil modification by termites in a sandy-soil vegetation in the Brazilian Atlantic rain forest. *J. Trop. Ecol.* **29**, 439–448 (2013).
- Oliveira, J. S. *et al.* Soil properties governing phosphorus adsorption in soils of Southern Brazil. *Geoderma Reg.* **22**, e00318 (2020).
- Freitas, D. F. *et al.* Pedogeomorphology and paleoenvironmental implications of large termite mounds at the Brazilian semiarid landscape. *Geomorphology* **387**, 107762 (2021).
- Antonello, A. A. Mineralogy of the deferrified clay fraction in B horizon of pedons of the VIIIITH International Soil Classification Workshop. In *Classification, Characterization and Utilization of Oxisols, Part 1: Papers. Proceedings of the Eight International Soil Classification Workshop, Brazil, SNLCS-Embrapa* (eds Beinroth, F. H. *et al.*) 109–138 (Soil Management Support Services and Soil Conservation Service—United States Department of Agriculture, University of Puerto Rico, 1988).
- Ker, J. C. & Resende, M. Caracterização química e mineralógica dos solos brunos subtropicais do Brasil. *R. Bras. Cienc. Solo* **14**, 215–225 (1990).
- Pereira, T. T. C. *et al.* Genesis of latosols and cambisols developed from pelitic rocks of the Bambui group, Minas Gerais state, Brazil. *R. Bras. Ci. Solo* **34**, 1283–1295 (2010).
- Reatto, A. *et al.* Geochemical processes in Latosols on the geomorphic surfaces from Brazilian Central Plateau. In *19th World Congress of Soil Science, Soil Solutions for a Changing World, 1–6 August 2010, Brisbane, Australia* (2010).
- Bertolazi, V. T. *et al.* Impact of an integrated no-till soybean-beef cattle production system on Oxisol mineralogy in southern Brazil. *Appl. Clay Sci.* **149**, 67–74 (2017).
- Pacheco, A. A. *et al.* Mineralogy, micromorphology and genesis of soils with varying drainage along a hillslope on granitic rocks of a Atlantic forest biome, Brazil. *R. Bras. Ci. Solo* **42**, e0170291 (2018).
- Almeida, C. C., Fontes, M. P. F., Dias, A. C., Pereira, T. T. C. & Ker, J. C. Mineralogical, chemical and electrochemical attributes of soils. *Sci. Agric.* **78**, e20200071 (2021).
- Reatto, A. *et al.* Variation of the kaolinite and gibbsite content at regional and local scale in the Latosols of the Brazilian Central Plateau. *C. R. Geosci.* **340**, 741–748 (2008).
- Jouquet, P. *et al.* Termites: The neglected soil engineers of tropical soils. *Soil Sci.* **181**, 157–165 (2016).
- Mujinya, B. B. *et al.* Clay composition and properties in termite mounds of the Lubumbashi area, D.R. Congo. *Geoderma* **192**, 304–315 (2013).
- Poss, R., Fardeau, J. C., Saragoni, H. & Quantin, P. Potassium release and fixation in Ferralsols (Oxisols) from Southern Togo. *J. Soil Sci.* **42**, 649–660 (1991).

42. Darunsontaya, T., Suddhiprakarn, A., Kheoruenromne, I. & Gilkes, R. J. The forms and availability to plants of soil potassium as related to mineralogy for upland Oxisols and Ultisols from Thailand. *Geoderma* **170**, 11–24 (2012).
43. Holt, A. J. & Lepage, M. Termites and soil properties. In *Termites: Evolution, Sociality, Symbioses, Ecology* Vol. 18 (eds Abe, T. *et al.*) 389–407 (Kluwer Academic Publishers, 2000).
44. Van Thuyne, J. & Verrecchia, E. P. Impacts of fungus-growing termites on surficial geology parameters: A review. *Earth-Sci. Rev.* **223**, 103862 (2021).
45. Jouquet, P., Traoré, S., Choosai, C., Hartmann, C. & Bignell, D. Influences of termites on ecosystem functioning Ecosystem services provided by termites. *Eur. J. Soil Biol.* **47**, 215–222 (2011).
46. Evans, T. A., Dawes, T. Z., Ward, P. R. & Lo, N. Ants and termites increase crop yield in a dry climate. *Nat. Commun.* **2**, 262 (2011).
47. Fernandes, G. W. *et al.* Afforestation of savannas: An impending ecological disaster. *Natureza Conservacao* **14**, 146–151 (2016).
48. King, L. C. A geomorfologia do Brasil Central. *R. Bras. Geogr.* **18**, 3–39 (1956).
49. Motta, P. E. F. *et al.* Relações solo-superfície geomórfica e evolução da paisagem em uma área do Planalto Central Brasileiro. *Pesq. Agropec. Bras.* **37**, 869–878 (2002).
50. Marques, J. J., Schulze, D. G., Curi, N. & Mertzman, S. A. Major element geochemistry and geomorphic relationships in Brazilian Cerrado soils. *Geoderma* **119**, 179–195 (2004).
51. Köppen, W. P. *Grundriss der Klimakunde* (Walter de Gruyter, 1931).
52. Assad, E. D., Sano, E. E., Masutomo, R., Castro, L. H. R. & Silva, F. A. M. Veranicos na região dos cerrados brasileiros: frequência e probabilidade de ocorrência. *Pesq. Agropec. Bras.* **28**, 993–1002 (1993).
53. Reatto, A., Bruand, A., Silva, E. M., Martins, E. S. & Brossard, M. Hydraulic properties of the diagnostic horizon of Latosols of a regional toposequence across the Brazilian Central Plateau. *Geoderma* **139**, 51–59 (2007).
54. Balbino, L. C. *et al.* Change in porosity and microaggregation in clayey Ferralsols of Brazilian Cerrado on clearing for pasture. *Eur. J. Soil Sci.* **53**, 219–230 (2002).
55. Balbino, L. C. *et al.* Change in hydraulic properties of a Brazilian clay Ferralsol on clearing for pasture. *Geoderma* **120**, 297–307 (2004).
56. Campos, J. E. G. Geologia do Distrito Federal. In *Zoneamento Ecológico-Econômico do Distrito Federal. SEDAH/ GDF. Subproduto 3.1* (2012).
57. Campos, J. E. G., Dardenne, M. A., Freitas-Silva, F. H. & Martins-Ferreira, M. A. C. Geologia do Grupo Paranoá na porção externa da Faixa Brasília. *Braz. J. Geol.* **43**, 461–476 (2013).
58. Bruand, A., Cousin, I., Nicoulaud, B., Duval, O. & Bégon, J. C. Backscattered electron scanning images of soil porosity for analyzing soil compaction around roots. *Soil Sci. Soc. Am. J.* **60**, 895–901 (1996).
59. Velde, B. & Meunier, A. *The Origin of Clay Minerals in Soils and Weathered Rocks* (Springer, 2008).
60. Arousseau, P., Curmi, P., Bouille, S. & Charpentier, S. Les vermiculites hydroxy-alumineuses du Massif Armoricaïn (France). Approche minéralogique, microanalytique et thermodynamique. *Geoderma* **31**, 17–40 (1983).

## Acknowledgements

The authors would like to thank Ida Di Carlo (CNRS) for managing the SEM/EDS equipment as well as providing expert advice on the chemical analyses recorded. They thank Christian Le Lay (INRAE) for impregnating the samples, Sylvain Janiec (University of Orléans) for preparing top quality polished sections and his technical assistance with Patricia Benoist-Juliot (CNRS) during observation and analysis sessions with the SEM/EDS. They acknowledge the pedology and geomorphology group of Embrapa Cerrados for its expertise for locating the soils to be sampled and its support in the field during sample collection and in the laboratory for routine characterization of the soil collected. This research is part of the Embrapa Cerrados–IRD Project No. 0203205 (Mapping of the Biome Cerrado Landscape and Functioning of Representative Soils). Finally, the authors acknowledge also financial support from the LabEx VOLTAIRE (LABX-100-01) project.

## Author contributions

All authors conceived and designed the study. A.R. and E.d.S.M. performed the field sampling. A.B. and A.R. carried out data acquisition. All authors substantially discussed the results and contributed to editing the manuscript.

## Competing interests

The authors declare no competing interests.

## Additional information

**Supplementary Information** The online version contains supplementary material available at <https://doi.org/10.1038/s41598-022-21613-6>.

**Correspondence** and requests for materials should be addressed to A.B.

**Reprints and permissions information** is available at [www.nature.com/reprints](http://www.nature.com/reprints).

**Publisher's note** Springer Nature remains neutral with regard to jurisdictional claims in published maps and institutional affiliations.



**Open Access** This article is licensed under a Creative Commons Attribution 4.0 International License, which permits use, sharing, adaptation, distribution and reproduction in any medium or format, as long as you give appropriate credit to the original author(s) and the source, provide a link to the Creative Commons licence, and indicate if changes were made. The images or other third party material in this article are included in the article's Creative Commons licence, unless indicated otherwise in a credit line to the material. If material is not included in the article's Creative Commons licence and your intended use is not permitted by statutory regulation or exceeds the permitted use, you will need to obtain permission directly from the copyright holder. To view a copy of this licence, visit <http://creativecommons.org/licenses/by/4.0/>.

© The Author(s) 2022